

Supporting Information

P-doped spherical hard carbon with high initial Coulombic efficiency and enhanced capacity for sodium ion batteries

Zheng-Guang Liu^{a,‡}, Jia-Hua Zhao^{a,b,‡}, Hao Yao^{a,b}, Xiang-Xi He^{a,b}, Hang Zhang^{a,b}, Yun Qiao^a, Xing-Qiao Wu^b, Li Li^{a,c*}, and Shu-Lei Chou^{b*}

a School of Environment and Chemical Engineering, Shanghai University, Shanghai 20444, P.R.China

b Institute for Carbon Neutralization, College of Chemistry and Materials Engineering, Wenzhou University, Wenzhou, Zhejiang 325035, P.R. China.

c Key Laboratory of Advanced Energy Materials Chemistry (Ministry of Education), Nankai University, Tianjin 300071, P.R.China

*Corresponding author

Email: LiLi2020@shu.edu.cn; chou@wzu.edu.cn

‡These authors contributed equally to this work.

1 Experimental Section

1.1 Material Synthesis.

All chemicals were used without any further purification. Glucose and phytic acid (PA 50 wt% in H₂O) were obtained from Aladdin Industrial Corporation. In a simple procedure, 0.9g glucose was dissolved in 50 ml deionized water under magnetic stirring for 30 min. Then a certain amount of phytic acid was added and stirred to form a homogeneous solution. Subsequently, the above solution was transferred in an autoclave (100 ml) and treatment at 200°C for 24h. After washing and drying processes, the dried precursors were put in to a tubular furnace. The temperature was firstly increased to 300 °C for 3h at a slow heating rate of 3 °C min⁻¹ and then increased to 1400 °C for 3h under Argon atmosphere. In this way, HC-PA with the mole ratio of glucose to PA 1:0.1,1:0.2,1:0.4 were obtained and the yielded PHC samples were labeled as PHC-0.1, PHC-0.2, PHC-0.4. For comparison, non-doped hard carbon spheres (HC) were also prepared with the same procedure except for removing PA in the precursor mixing step.

Synthesis of Na₂Fe_{0.5}Mn_{0.5}[Fe(CN)₆](FeMnHCF) : 22.5 mmol MnSO₄·H₂O, 22.5 mmol FeSO₄·7H₂O, 180 mmol sodium citrate and 4 mmol ascorbic acid were dissolved in 100 mL deionized water to form solution A. 45 mmol Na₄Fe(CN)₆·10H₂O dissolved in 100 mL deionized water to form solution B. After then, solution A and solution B were mixed, stirred under magnetic stirring for 8 hours at 45°C, and then aged for 24 hours at 45°C. The precipitates were collected by centrifugation, washed for three times with deionized water and ethanol. Finally, the products were obtained after drying in a vacuum oven at 120°C.

1.2 Material characterization

The morphologies of the obtained materials were analyzed by scanning electron microscopy (SEM) with instrument HITACHI SU-1500. A high-resolution transmission electron microscope (HR-TEM, JEOL-2100F) was used to analyze the

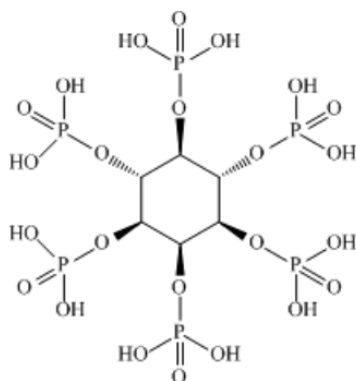
detailed crystal structure of the material. X-ray diffraction (XRD, 18KW D/MAX2500V) was used to confirm crystalline structures of the obtained materials. Raman spectra were recorded with a Renishaw in Via instrument equipped with a 532 nm wavelength laser. The specific surface area and pore structure analysis of the material was characterized by nitrogen adsorption-desorption measurement (ASAP 2460, Micromeritics, USA). X-ray photoelectron (XPS) were obtained by an X-ray photoelectron spectrometer (Thermo Scientific K-Alpha) with an excitation source of Al K α radiation (1486.6 eV). Operando Raman spectroscopy equipment was provided by Beijing SciStar Technology Co. Ltd. The charge and discharge curves versus time of the in-situ cell were controlled by the chronopotentiometry facility on a CHI660E electrochemical workstation. The potential range was from open-circuit voltage (OCV) to 0.003 V. Scan interval: 434 s. Total test: 80 points. Exposure time: 10 s. Laser power: 50%. Accumulation: 20 times. All electrochemical tests were carried out at room temperature.

1.3 Electrochemical measurement

The anode was fabricated from the active materials and sodium alginate binder, which were blended at ratios of 95:5 in deionized water. After forming a slurry, the mixture was coated on copper foil and dried at 100 °C in a vacuum for 12 h. The Cu foil with active material was cut into disk electrodes. The loading of active materials in electrodes is about 1.5-2 mg cm⁻². The CR2032 coin cells were assembled in an argon-filled glove box with O₂ and H₂O at less than 0.01 ppm. The electrode sheet was used as the working electrode, the sodium metal as the counter electrode, glass fiber (GF/A, Whatman, UK) as separator and the electrolyte was 1M NaPF₆ in 1:1 EC/DMC. For the assembly of full cell, PHC-0.2 was firstly presodiated through simple contact with the sodium foil as the anode, and Na₂Fe_{0.5}Mn_{0.5}[Fe(CN)₆] (FeMnHCF) was as the cathode. Separator was the glass fiber (16 mm in diameter, GF/A Glass fiber filters, Whatman). 100 μ L of electrolytes were used for the whole cell. The full cells were charged and discharged at 50 mA g⁻¹ from 2 to 3.6 V vs Na⁺/Na. The current densities

were normalized by the active mass of the carbon anode. Cyclic Voltammograms (CV) was conducted on electrochemical workstation (CHI660E) at the scanning rate of 0.1 mV s⁻¹. The galvanostatic charge and discharge testing was carried out on a LAND CT2001 battery test system in the voltage range of 0~2.5 V at room temperature on a Land-CT2001A tester, GITT tests were carried out with a galvanostatic density of 20 mA g⁻¹ pulsed for 10 minutes and then rest intervals for 30 min intervals until the set voltage was reached. The electrochemical impedance spectroscopy (EIS) was measured from 100 kHz to 0.1 Hz.

2 Supplementary Figures and Tables



Scheme. S1 Chemical formula of phytic acid(PA).

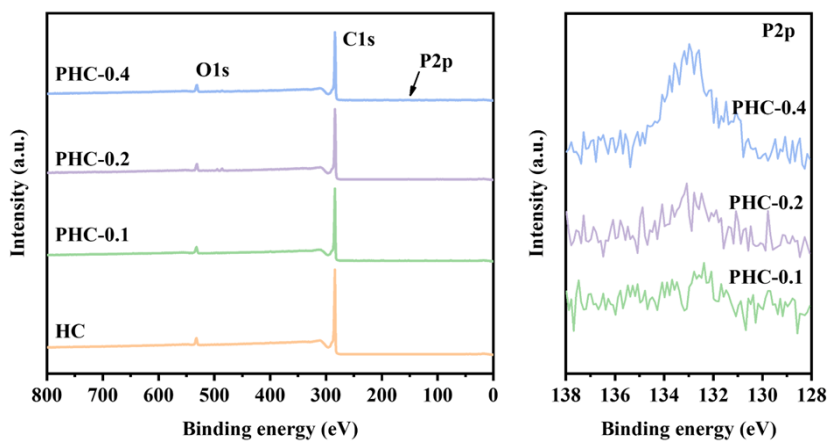


Fig. S1 X-ray photoelectron spectroscopy survey scan profiles of the P-doped.

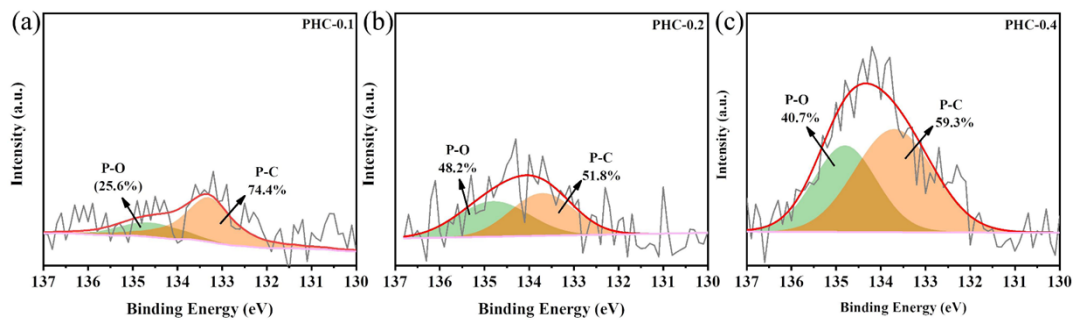


Fig. S2 P 2p spectra of PHC-0.1, PHC-0.2 and PHC-0.4

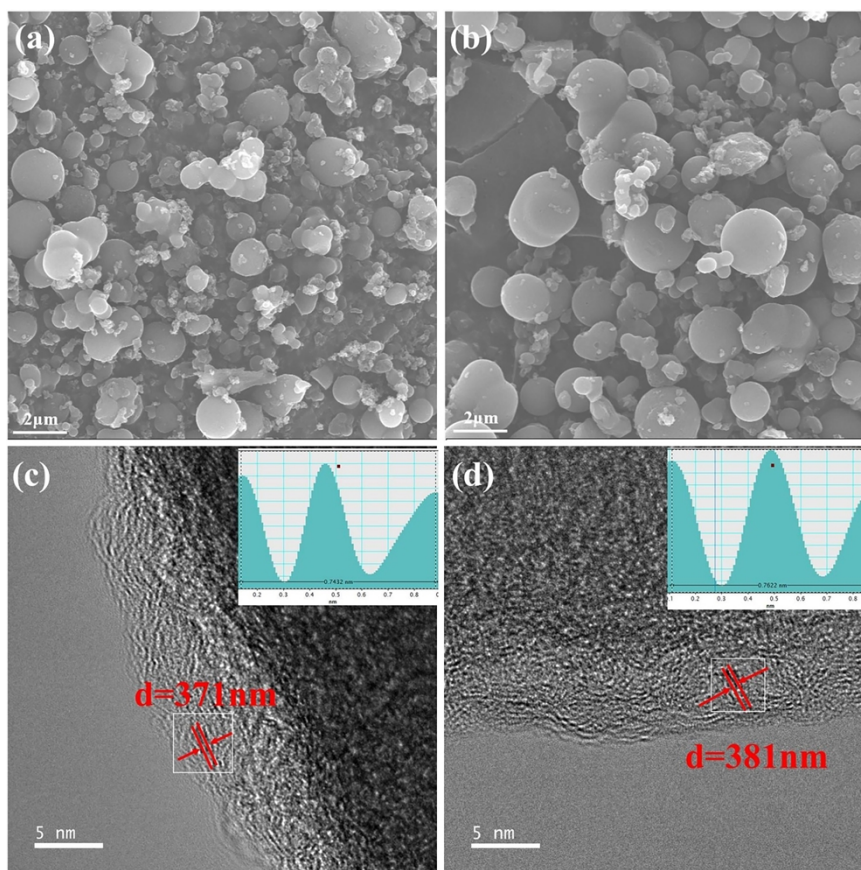


Fig. S3 SEM images of (a)PHC-0.1 and (b)PHC-0.4.HRTEM images of (c) PHC-0.1 and (d)

PHC-0.4

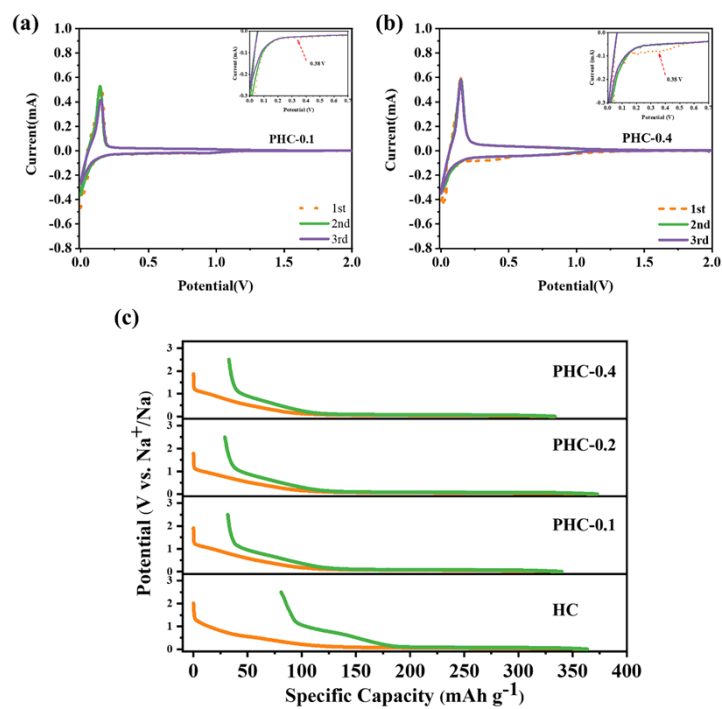


Fig. S4 The CV curves of (a)PHC-0.1;(b) PHC-0.4 and (c)Initial galvanostatic charge–discharge profiles of the HC and PHC-X electrodes at 20 mA g⁻¹.

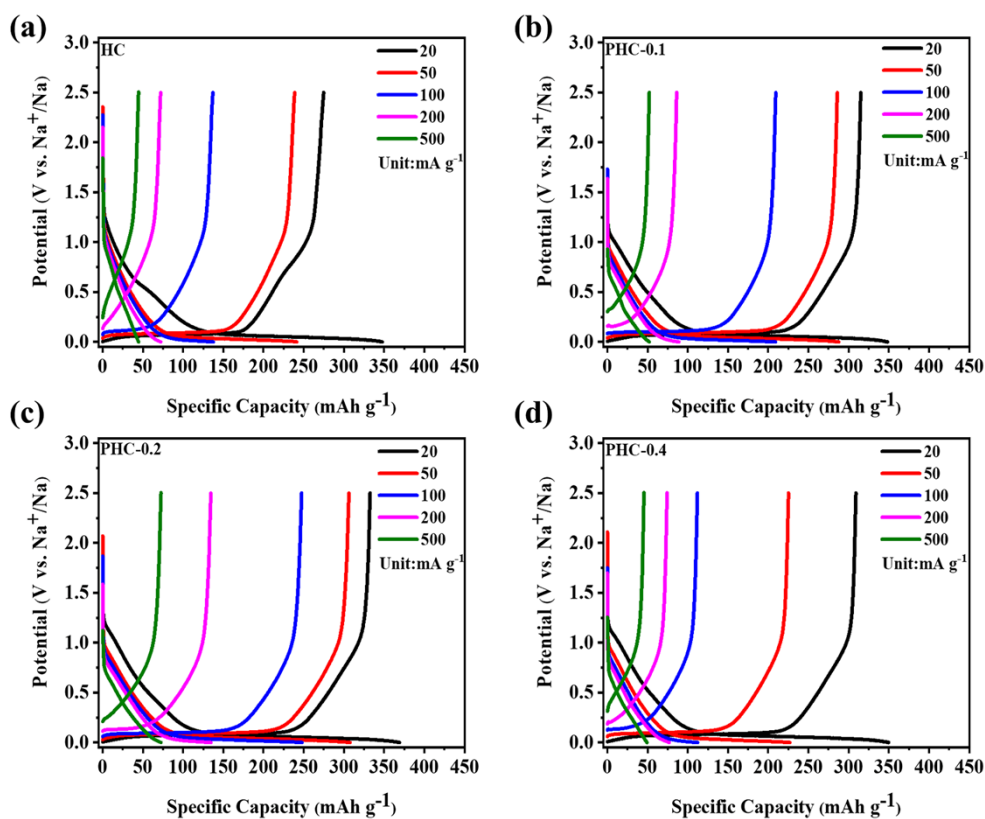


Fig. S5 Discharge-charge profiles of PHC-X anode at different current densities.

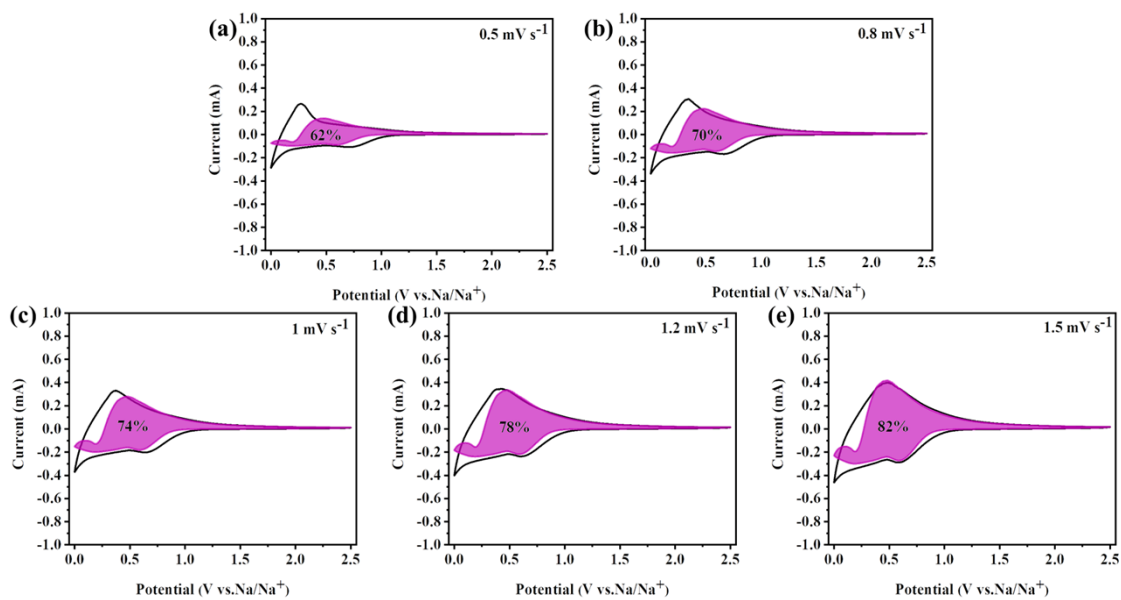


Fig. S6 Capacitive contribution ratios at different scan rates of (a) 0.5, (b) 0.8, (c) 1.0, (d) 1.2 and (e) 1.5 mV s^{-1} .

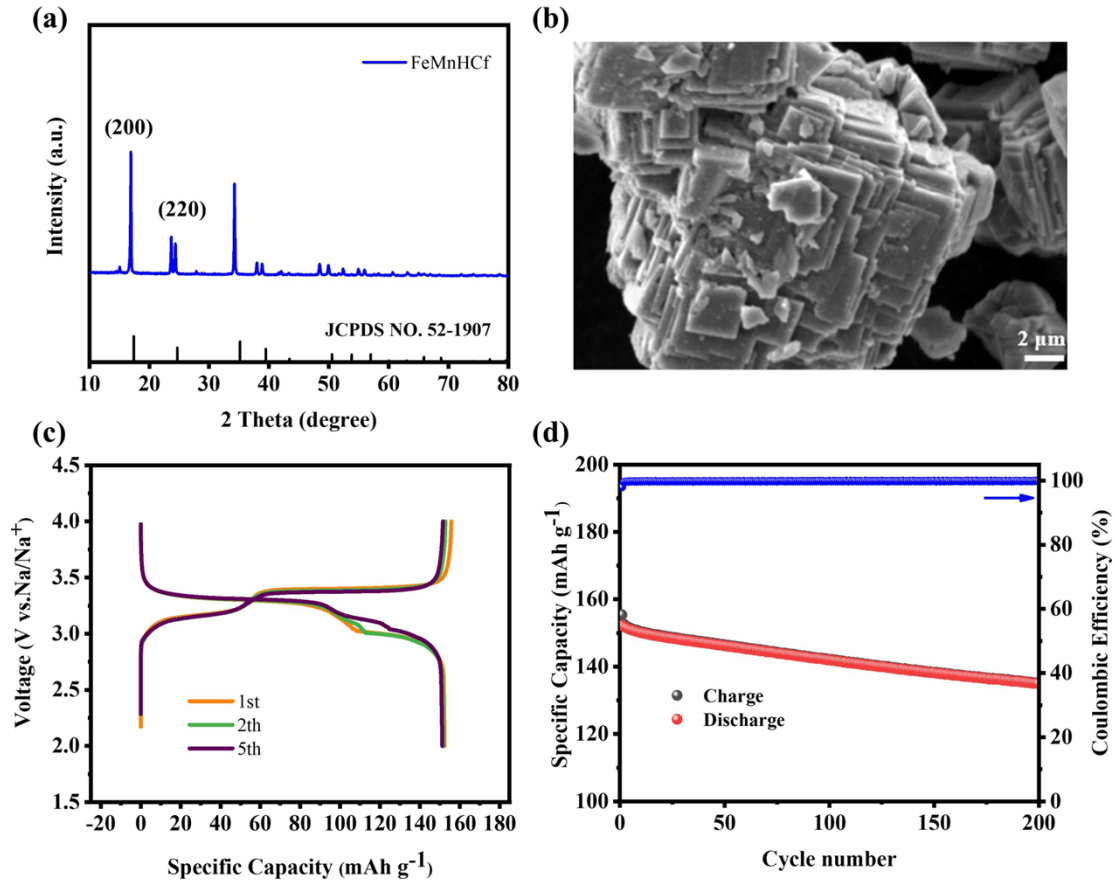


Fig. S7 Structural, morphological and electrochemical characterizations of $\text{Na}_2\text{Fe}_{0.5}\text{Mn}_{0.5}[\text{Fe}(\text{CN})_6](\text{FeMnHCF})$ cathode. (a) XRD, (b) SEM, (c) and (d) charge-discharge profile and cyclic stability at a constant current of 50 mA g^{-1}

Table. S1 Comparison of the ICE, total capacity, plateau capacity and pyrolysis temperature of heteroatom doped carbons in SIB.

Doping	Materials	Pyrolysis Temperature (°C)	Total capacity (mAh g^{-1})	Plateau capacity (mAh g^{-1})	ICE(%)	Refs.
N	N-doped biomass carbon/reduced graphene oxide (NC/RGO) composite	800	395 at 0.1 A g^{-1} .	None	40.1	1
	N-doped hollow porous carbon microspheres (NHPCS)	850	337.5 at 0.1 A g^{-1}	None	27	2
	N-doped Porous Hard-Carbon	900	190 at 20 mA g^{-1}	None	/	3
	N-doped porous carbon (NPC)	700	421 at 50 mA g^{-1}	None	47.8	4
	Nitrogen-rich mesoporous carbon	700	338 at 30 mA g^{-1}	70 at 30 mA g^{-1}	54	5
P	Phosphorus-doped hard carbon	700	379.3 at 0.1 A g^{-1}	None	≈ 47	6
	Phosphorus-doped hard carbon	1000	288 at 50 mA g^{-1}	54 at 50 mA g^{-1}	56	7

nanofibers						
S	Ultra-high phosphorus-doped carbon	700	500.9 at 0.1 A g ⁻¹	None	71.5	8
	Sulfur-doped graphene (S-SG)	500	488 at 0.1 A g ⁻¹	None	55.6	9
	S-doped hard carbon material	500	948 at 0.1 A g ⁻¹	None	84.4	10
Co-doping	S-doped hard carbon	1100	328 at 20 m A g ⁻¹	177 at 20 m A g ⁻¹	80.3	11
	Sulfur and nitrogen co-doped hierarchically porous carbon materials (SN-HPCS)	800	680 at 0.8 A g ⁻¹	None	33.7	12
	Nitrogen and phosphorus co-doped porous carbon (NPPC)	900	423 at 50 m A g ⁻¹	None	42.8	13
	N, P co-doped carbon microspheres(NPCM)	800	350 at 50 m A g ⁻¹	32 at 50 m A g ⁻¹	≈47	14

Table. S2. Calculation results of XRD. XRD, X-ray diffraction Bragg equation

$$d_{002} = \lambda / 2 \sin \theta_{002}$$

where λ is the wavelength of the X-rays (0.154 nm), $2\theta_{002}$ is the peak position of (002) peak in the XRD pattern.

Scherer equation

$$L_a = 1.84\lambda / B_{101} \cos \theta_{100}$$

$$L_c = 0.89\lambda / B_{002} \cos \theta_{002}$$

where λ is the wavelength of the X-rays (0.154 nm), B_{101} and B_{002} are the full width at half maxima of the (101) and (002) peaks, $2\theta_{101}$ and $2\theta_{002}$ are the corresponding peak positions.

Samples	$2\theta_{(002)}$ (°)	$d_{(002)}$ (nm)	B_{002} (°)	L_c (nm)	$2\theta_{(101)}$ (°)	$d_{(101)}$ (nm)	B_{101} (°)	L_a, XRD (nm)	A_{D1}/A_G
HC	23.46	0.378	7.51	1.06	43.74	0.206	4.271	4.095	1.006
PHC-0.1	23.36	0.380	7.42	1.08	43.63	0.207	4.302	4.064	1.025
PHC-0.2	23.23	0.382	7.41	1.08	43.00	0.210	4.292	4.064	1.050
PHC-0.4	23.20	0.383	7.99	1.00	43.77	0.206	4.293	4.075	1.064

Table. S3 Physical parameters obtained by N₂ adsorption-desorption

	BET surface area	Total pore	Micropore	Average pore
	(m² g⁻¹)	volume(cm³ g⁻¹)	volume(cm³ g⁻¹)	diameter(nm)
HC	156.37	0.086	0.054	1.9668
PHC-0.1	81.26	0.049	0.027	1.9923
PHC-0.2	44.31	0.028	0.013	2.0956
PHC-0.4	88.10	0.080	0.026	2.7101

Table. S4 Comparison of the ICE of various carbonaceous anode materials in SIBs.

Materials	Electrolyte	Current density	ICE	Year	Refs
		(mA·g⁻¹)			
golden berry leaves	1 M NaClO ₄ in EC/DMC	20	86.43%	2021	15
buckwheat hulls	1 M NaClO ₄ in EC/DEC (2%FEC)	50	72%	2020	16
Lignin-derived hard carbon microspheres	1 M NaClO ₄ in EC/DEC	25	82%	2020	17
lignin-based resin spheres	1 M NaPF ₆ in EC/DEC (5% FEC)	25	74%	2020	18
lignite-derived hard carbons	1 M NaClO ₄ in EC/DEC	20	83%	2020	19
the porous carbon microspheres	1 M NaClO ₄ in EC/DEC(5%FEC)	100	44.1%	2021	20
a core-shell Co ₂ VO ₄ / carbon composite	1 M NaClO ₄ in EC/DMC (5%FEC)	100	~37%	2021	21
binder and current collector-free hard carbon	1 M NaClO ₄ in EC/DEC	37.2	85%	2020	22
Hard-soft carbon composites	1 M NaClO ₄ in EC/DMC	30	80%	2019	23

References

- 1 R. Dan, W. Chen, Z. Xiao, P. Li, M. Liu, Z. Chen and F. Yu, *Energy Fuels*, 2020, **34**, 3923.
- 2 X. Wang, F. Zhu, M. Xiao, S. Liu, X. Liu and Y. Meng, *J Mater Sci: Mater Electron*, 2022, **33**, 7913.
- 3 Y. Wang, Y. Li, S. S. Mao, D. Ye, W. Liu, R. Guo, Z. Feng, J. Kong and J. Xie, *Sustainable Energy & Fuels*, 2019, **3**, 717.
- 4 G. Zeng, B. Zhou, L. Yi, H. Li, X. Hu and Y. Li, *Sustainable Energy & Fuels*, 2018, **2**, 855.
- 5 H. Liu, M. Jia, N. Sun, B. Cao, R. Chen, Q. Zhu, F. Wu, N. Qiao and B. Xu, *ACS Appl Mater Interfaces*, 2015, **7**, 27124.
- 6 N. Li, Q. Yang, Y. Wei, R. Rao, Y. Wang, M. Sha, X. Ma, L. Wang and Y. Qian, *J. Mater. Chem. A*, 2020, **8**, 20486.
- 7 F. Wu, R. Dong, Y. Bai, Y. Li, G. Chen, Z. Wang and C. Wu, *ACS Appl Mater Interfaces*, 2018, **10**, 21335.
- 8 J. Yan, H. Li, K. Wang, Q. Jin, C. Lai, R. Wang, S. Cao, J. Han, Z. Zhang, J. Su and K. Jiang, *Adv. Energy Mater.*, 2021, **11**, 2003911.
- 9 B. Quan, A. Jin, S.-H. Yu, S. M. Kang, J. Jeong, H. D. Abruña, L. Jin, Y. Piao and Y.-E. Sung, *Adv. Sci.*, 2018, **5**, 1700880.
- 10 B. Wan, H. Zhang, S. Tang, S. Li, Y. Wang, D. Wen, M. Zhang and Z. Li, *Sustainable Energy & Fuels*, 2022, **6**, 4338.
- 11 Z. Li, C. Bommier, Z. S. Chong, Z. Jian, T. W. Surta, X. Wang, Z. Xing, J. C. Neuefeind, W. F. Stickle, M. Dolgos, P. A. Greaney and X. Ji, *Adv. Energy Mater.*, 2017, **7**, 1602894.
- 12 L. He, W. Sun, K. Sun, Y. Mao, T. Deng, L. Fang, Z. Wang and S. Chen, *J. Power Sources*, 2022, **526**, 231019.

- 13 C. Chen, Y. Huang, Z. Meng, M. Lu, Z. Xu, P. Liu and T. Li, *Journal of Materials Science & Technology*, 2021, **76**, 11.
- 14 Y. Li, Z. Wang, L. Li, S. Peng, L. Zhang, M. Srinivasan and S. Ramakrishna, *Carbon*, 2016, **99**, 556.
- 15 R.-R. Li, X.-X. He, Z. Yang, X.-H. Liu, Y. Qiao, L. Xu, L. Li and S.-L. Chou, *Mater. Chem. Front.*, 2021, **5**, 7595.
- 16 C. Chen, Y. Huang, Y. Zhu, Z. Zhang, Z. Guang, Z. Meng and P. Liu, *ACS Sustain. Chem. Eng.*, 2020, **8**, 1497.
- 17 J. Zhang, B. Yu, Y. Zhang and C. Wang, *Energy Tech*, 2020, **8**, 1901423.
- 18 Y. Zhang, Y. Zhu, J. Zhang, S. Sun, C. Wang, M. Chen and J. Zeng, *Energy Tech*, 2020, **8**, 1900694.
- 19 Y. Zou, H. Li, K. Qin, Y. Xia, L. Lin, Y. Qi, Z. Jian and W. Chen, *J Mater Sci*, 2020, **55**, 5994.
- 20 S. Chen, K. Tang, F. Song, Z. Liu, N. Zhang, S. Lan, X. Xie and Z. Wu, *Nanotechnology*, 2021, **33**.
- 21 C. Wang, Z. Wang, D. Zhao, J. Ren, S. Liu, H. Tang, P. Xu, F. Gao, X. Yue, H. Yang, C. Niu, W. Chu, Di Wang, X. Liu, Z. Wang, Y. Wu and Y. Zhang, *ACS Appl Mater Interfaces*, 2021, **13**, 55020.
- 22 A. Beda, C. Villevieille, P.-L. Taberna, P. Simon and C. Matei Ghimbeu, *J. Mater. Chem. A*, 2020, **8**, 5558.
- 23 F. Xie, Z. Xu, A. C. S. Jensen, H. Au, Y. Lu, V. Araullo-Peters, A. J. Drew, Y.-S. Hu and M.-M. Titirici, *Adv Funct Materials*, 2019, **29**, 1901072.
- 24 A. Kamiyama, K. Kubota, T. Nakano, S. Fujimura, S. Shiraishi, H. Tsukada and S. Komaba, *ACS Appl. Energ. Mater.*, 2020, **3**, 135.